JOURNAL OF SYNCHROTRON RADIATION
ISSN 1600-5775

Identification of Ca-rich dense granules in human platelets using scanning transmission X-ray microscopy

Tung X. Trinh,[a] Sook Jin Kwon,[b] Zayakhuu Gerelkhuu,[b] Jang Sik Choi,[b,c] Jaewoo Song[d] and Tae Hyun Yoon[a,b,c]*

[a]Department of Chemistry, College of Natural Sciences, Hanyang University, Seoul 04763, Republic of Korea, [b]Center for Next Generation Cytometry, Hanyang University, Seoul 04763, Republic of Korea, [c]Institute of Next Generation Material Design, Hanyang University, Seoul 04763, Republic of Korea, and [d]Department of Laboratory Medicine, College of Medicine, Yonsei University, Seoul 03722, Republic of Korea. *Correspondence e-mail: taeyoon@hanyang.ac.kr

Received 16 September 2019
Accepted 26 February 2020

Edited by S. M. Heald, Argonne National Laboratory, USA

Keywords: platelets; dense granules; STXM; calcium mapping.

Whole-mount (WM) platelet preparation followed by transmission electron microscopy (TEM) observation is the standard method currently used to assess dense granule (DG) deficiency (DGD). However, due to the electron-density-based contrast mechanism in TEM, other granules such as α-granules might cause false DG detection. Here, scanning transmission X-ray microscopy (STXM) was used to identify DGs and minimize false DG detection of human platelets. STXM image stacks of human platelets were collected at the calcium (Ca) $L_{2,3}$ absorption edge and then converted to optical density maps. Ca distribution maps, obtained by subtracting the optical density maps at the pre-edge region from those at the post-edge region, were used to identify DGs based on the Ca richness. DGs were successfully detected using this STXM method without false detection, based on Ca maps for four human platelets. Spectral analysis of granules in human platelets confirmed that DGs contain a richer Ca content than other granules. The Ca distribution maps facilitated more effective DG identification than TEM which might falsely detect DGs. Correct identification of DGs would be important to assess the status of platelets and DG-related diseases. Therefore, this STXM method is proposed as a promising approach for better DG identification and diagnosis, as a complementary tool to the current WM TEM approach.

1. Introduction

Platelets are small discoid-shaped anuclear blood cells, which are well known as essential components in haemostasis, the process of preventing blood loss through injured blood vessels. They contain several types of subcellular structures, including α-granules and dense granules (DG). Amonsg these subcellular structures, a deficiency of DGs, as found in previous research into Hermansky–Pudlak syndrome (Nishibori *et al.*, 1993) and Chediak–Higashi syndrome (Introne *et al.*, 1999), would lead to bleeding diathesis. Evaluation of platelets by whole-mount transmission electron microscopy (WM TEM) is an essential step in diagnostic workup of dense-granule deficiency (DGD) and is now considered the gold-standard test for diagnosing DGDs (White, 1969, 1979, 1998, 2004; Hayward *et al.*, 2009, 2012; Brunet *et al.*, 2018; Chen *et al.*, 2018).

Unfortunately, however, TEM has some drawbacks for the characterization of platelet DGs. Generally, WM TEM measurements are conducted without staining the DGs, since the high contents of calcium (Ca) and phosphorus (P) in platelet DGs block the electron beam and create contrast. However, TEM shows its best spatial resolution for sample thicknesses less than ~100 nm, and WM TEM observation of

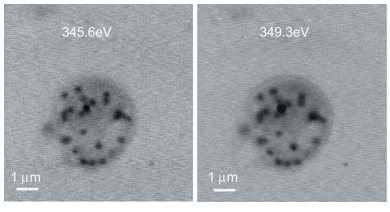

platelets with a variable thickness of 1–3 μm often results in defocused and blurred images of subcellular granules. Additionally, because of the electron-density-based contrast mechanism, other granules such as α-granules might cause false detection of DGs.

Recently, scanning transmission X-ray microscopy (STXM) has shown its capabilities and these may complement the current limitations of WM TEM by providing a better contrast mechanism and penetration depth with enough spatial resolution (Benzerara *et al.*, 2004; Nelson *et al.*, 2010; Kwon *et al.*, 2014; Yang *et al.*, 2014; Nho *et al.*, 2016; Nho & Yoon, 2017). In particular, the contrast mechanism of STXM, which is based on the difference in X-ray absorption at the pre- and post-edges, allows us to distinguish Ca-rich DGs, which may provide much clearer and more DG-specific contrast than the electron-density-based contrast of TEM. However, STXM studies of platelets in the soft X-ray region have not been reported yet. In this study, synchrotron-based STXM in the soft X-ray region has been adapted for the characterization of human platelet DGs, and its capability demonstrated of identifying and counting DGs in human platelets and diagnosing DGD.

2. Methods

2.1. Platelet sample preparation

Whole blood was obtained from normal healthy persons after informed consent, the study was approved by the Institutional Review Board of Yonsei Severance Hospital, Seoul, and all experiments were performed in accordance with relevant guidelines and regulations. Fresh platelet-rich plasma (PRP) was used for the STXM measurements.

Whole blood was drawn into tubes containing acid citrate dextrose (one-sixth of the volume of blood drawn). PRP was obtained by centrifugation at 210 × *g* for 15 min at 310 K. The fresh PRP was then washed five times using deionized water with the protocol of adding 800 μl of deionized water then centrifuging and removing 800 μl of the upper solution. A single drop of the remaining platelet solution (approximately 2 μl) was transferred to a Formvar-coated copper grid, followed by air-drying overnight. Any excess solution of fresh platelets was removed using filter paper. The copper grids containing the dried platelets were then used for STXM measurements.

2.2. STXM measurements

STXM images were acquired on beamline 10A at the Pohang Light Source (PLS; Pohang Accelerator Laboratory, Republic of Korea). The storage-ring current of 200 mA at the PLS was operated in top-up mode. The synchrotron-based monochromatic soft X-ray beam was focused to ∼25 nm using a Fresnel zone plate (outermost zone width of 25 nm). The first order of the diffractive focused X-ray beam was selected using the order-sorting aperture (OSA; pinhole diameter of 100 μm). The sample was mounted on an interferometrically controlled piezo stage and raster scanned. The intensity of the transmitted X-ray beam was measured using a scintillator photomultiplier tube (PMT). STXM images of whole-mounted platelets were collected for an area of 10 μm × 10 μm with 300 × 300 pixels. To obtain the Ca $L_{2,3}$ edge XANES spectra, stack images of platelets were collected in the energy range 345.6–355.6 eV. The energy position of the Ca L_3-edge and L_2-edge main peaks were calibrated to 349.3 and 352.6 eV, respectively, according to Rieger *et al.* (1986). The *aXis2000* software (Version 01-Oct-2018; Hitchcock, 2019) was used to calculate the optical density (OD) and Ca distribution maps.

3. Results and discussion

It has long been known that DGs contain high contents of Ca and P (White, 1979; Israels *et al.*, 1992; McNicol & Israels, 1999; Ruiz *et al.*, 2004; Lo *et al.*, 2005), making DGs electron dense and allowing them to be visualized without a special staining procedure. However, the electron-density-based contrast of WM TEM is not element-specific and there may be interference from the presence in the platelets of other subcellular granules with high-atomic-number elements, such as α-granules, which could cause errors in counting DGs and diagnosing DGD.

The high content of Ca was chosen in this STXM study to distinguish DGs from other subcellular granules. However, in contrast with the electron-density-based contrast mechanism of TEM, the STXM approach uses a more distinct contrast mechanism based on element- or chemical species-specific XANES (X-ray absorption near-edge structure) features, which allows a much clearer identification of platelet DGs. As shown in Fig. 1, STXM images of a whole-mounted platelet (platelet 1) were collected and converted to OD maps. Ca distribution maps were then obtained by subtracting the OD map at the pre-edge region from the OD map at the post-edge region. In the STXM images collected at energies of 345.6 and 349.3 eV [Figs. 1(*a*) and 1(*c*), respectively], many subcellular granules were observed with good contrast. When these images were converted to OD maps, one granule became even brighter in the OD image collected at 349.3 eV [Fig. 1(*d*)], while the other granules remained with similar contrast [Figs. 1(*b*) and 1(*d*)]. In the Ca distribution map shown in Fig. 1(*e*), only one granule was observed as a bright spot, while the others were mostly dimmed. This bright spot in Fig. 1(*e*) is a Ca-rich subcellular granule of platelets, which can be clearly identified as a DG.

Additionally, six different regions of this platelet [regions 1–6 of Fig. 1(*d*)] were chosen and their Ca $L_{2,3}$-edge XANES spectra are displayed in Fig. 1(*f*). A rectangular area outside of platelet 1 [Fig. 1(*d*)] was chosen for background subtraction of XANES spectra. The XANES spectrum of the brightest spot in the Ca map [region 1 of Fig. 1(*d*)] displays a typical Ca $L_{2,3}$-edge XANES spectrum, similar to those previously reported in the literature (Benzerara *et al.*, 2004; Naftel *et al.*, 2001; Obst *et al.*, 2009; Cosmidis *et al.*, 2015), with two strong (349.3 and 352.6 eV) and two weak (348.3 and 351.5 eV) absorption peaks, which might be due to the presence of Ca

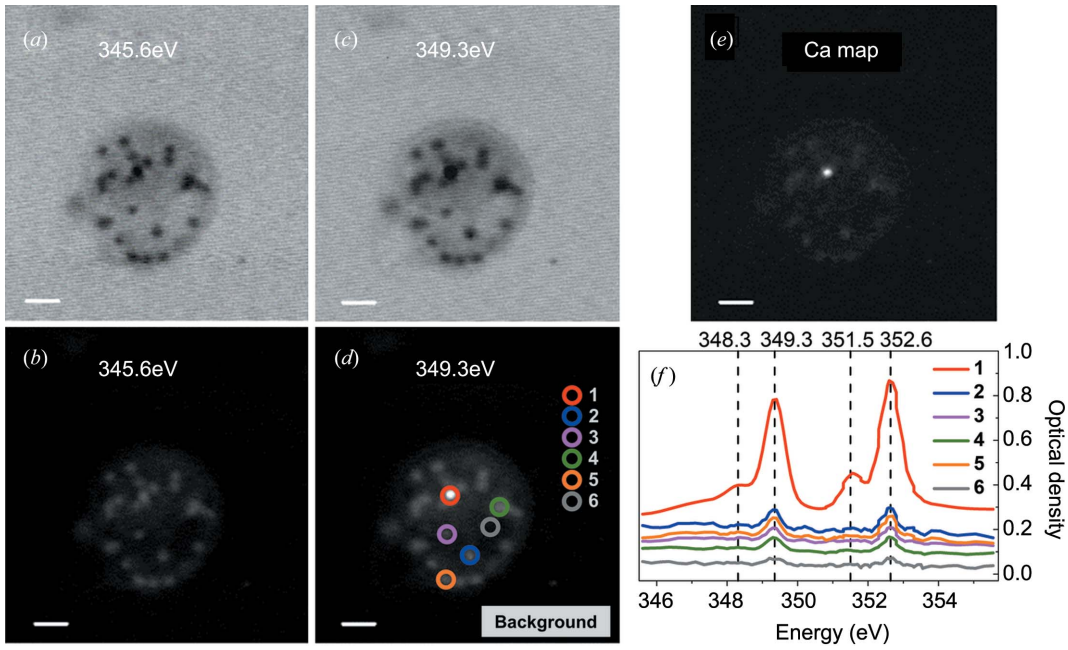

Figure 1
STXM transmission images at (*a*) 345.6 eV and (*c*) 349.3 eV. STXM OD images of platelet 1 at (*b*) 345.6 eV and (*d*) 349.3 eV. (*e*) A calcium map of platelet 1 obtained by subtracting (*b*) from (*d*). (*f*) XANES spectra of six regions inside platelet 1 [marked in panel (*d*)]. Scale bars are 1 µm.

species such as Ca gluconate, Ca glycerophosphate, Ca carbonate *etc.* (Naftel *et al.*, 2001; Fleet & Liu, 2009). The XANES spectra of the other four Ca granules [regions 2–5 of Fig. 1(*d*)] also display spectral features of Ca species but with much reduced intensities, indicating that these granules contain much smaller amounts of Ca. However, due to the low levels of Ca signal in these regions, it was not possible to identify clearly the Ca species for those low Ca-containing granules. A small absorption peak observed in the cytoplasm region of the platelet suggested that only a negligible amount of Ca was present in the cytoplasm of the platelet [region 6 of Fig. 1(*d*)]. With these Ca $L_{2,3}$-edge XANES spectra and the Ca distribution map, we could confirm that the brightest spot in the Ca map [Fig. 1(*e*)] was a DG, while the other particles, which were observed as bright spots in the OD map at 349.3 eV but found as dimmed in the Ca maps, were probably other types of subcellular granules.

We compare STXM and TEM images of the sample platelet in Fig. 2. The TEM image was obtained after STXM measurement. The four dark horizontal lines in the TEM image [Fig. 2(*c*)] were caused by STXM line scans for the collection of Ca $L_{2,3}$ spectra. Based on the Ca map of the platelet [Fig. 2(*a*)], there is only one DG in the platelet, as indicated by a red arrow. However, in the TEM image [Fig. 2(*c*)], which shows the same platelet as the STXM image [Fig. 2(*b*)], there are five dark particles having similar contrast and shape to a DG. Four of them were in platelet cytoplasm and they have the typical microscopic features of true DGs which were suggested by Chen *et al.* (2018): a uniformly dense texture, perfectly round with sharp contours, and larger than 50 nm in diameter. Therefore, it is possible to recognize these four particles incorrectly as DGs based only on the microscopic features of TEM images.

Further collection of STXM images was performed for three other platelets (platelets 2 to 4) and their original and processed STXM images are presented in Fig. 3. In the Ca distribution maps of these platelets, DGs are clearly distinguished as bright spots within the cytoplasm of the platelets

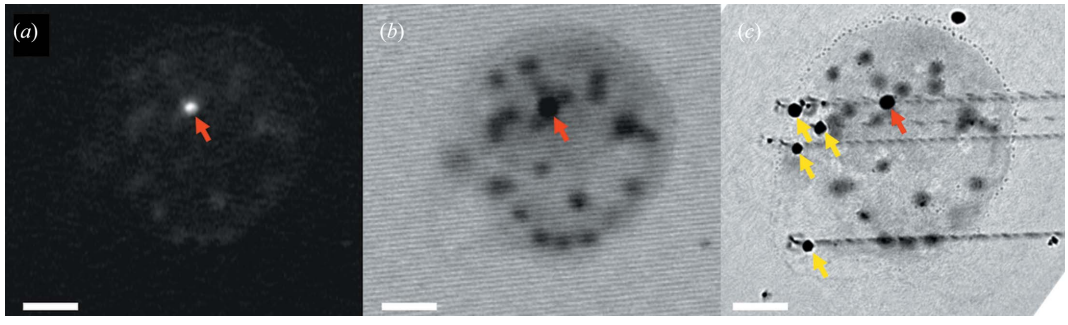

Figure 2
(*a*) The calcium map, (*b*) an STXM transmission image and (*c*) a TEM image of platelet 1. Red arrows indicate true DG detection and yellow arrows indicate false DG detection. The four dark horizontal lines in panel (*c*) are caused by line scans during STXM measurement for the collection of Ca $L_{2,3}$ spectra. Scale bars are 1 µm.

Table 1
Image analysis results for the DGs in STXM-based Ca maps for platelets 1 to 4.

Platelet No.	DGs identified	Area (μm^2)	Circularity	Feret diameter (μm)	Diameter based on circle shape (μm)	Average intensity in Ca map	Maximum intensity in Ca map
1	1	0.065	0.917	0.329	0.288	0.590 ± 0.294	1.137
2	1	0.024	0.904	0.216	0.175	0.176 ± 0.099	0.438
	2	0.026	0.897	0.247	0.182	0.173 ± 0.095	0.390
	3	0.018	0.897	0.204	0.151	0.224 ± 0.107	0.336
	4	0.021	1.000	0.204	0.164	0.232 ± 0.127	0.487
3	1	0.051	0.572	0.351	0.255	0.316 ± 0.128	0.560
	2	0.026	0.624	0.224	0.182	0.305 ± 0.083	0.487
4	1	0.024	0.944	0.199	0.175	0.326 ± 0.117	0.506

(Fig. 3, panels A5–D5). Further image analysis of the Ca maps of these platelets allowed us to extract additional parameters for the DGs, such as area, circularity, diameter and Ca content for each granule (Table 1). These parameters would be useful for the further development of image-based DG diagnosis models, as well as for image interpretation criteria.

Recently, Chen *et al.* (2018) proposed DG interpretation criteria for WM TEM images, in which three typical microscopic features of true DGs were described as a uniformly dense/dark texture, a perfectly round shape with sharp contours and a diameter larger than 50 nm. As a complementary approach to WM TEM, STXM-based Ca distribution maps may provide additional DG interpretation criteria that might refine and improve the accuracy of DGD diagnosis. However, since the number of platelets analysed in this 'proof of concept' study is limited, it is not currently feasible to extract quantitative criteria for the identification of DGs and the diagnosis of DGD patients. Follow-up studies with larger

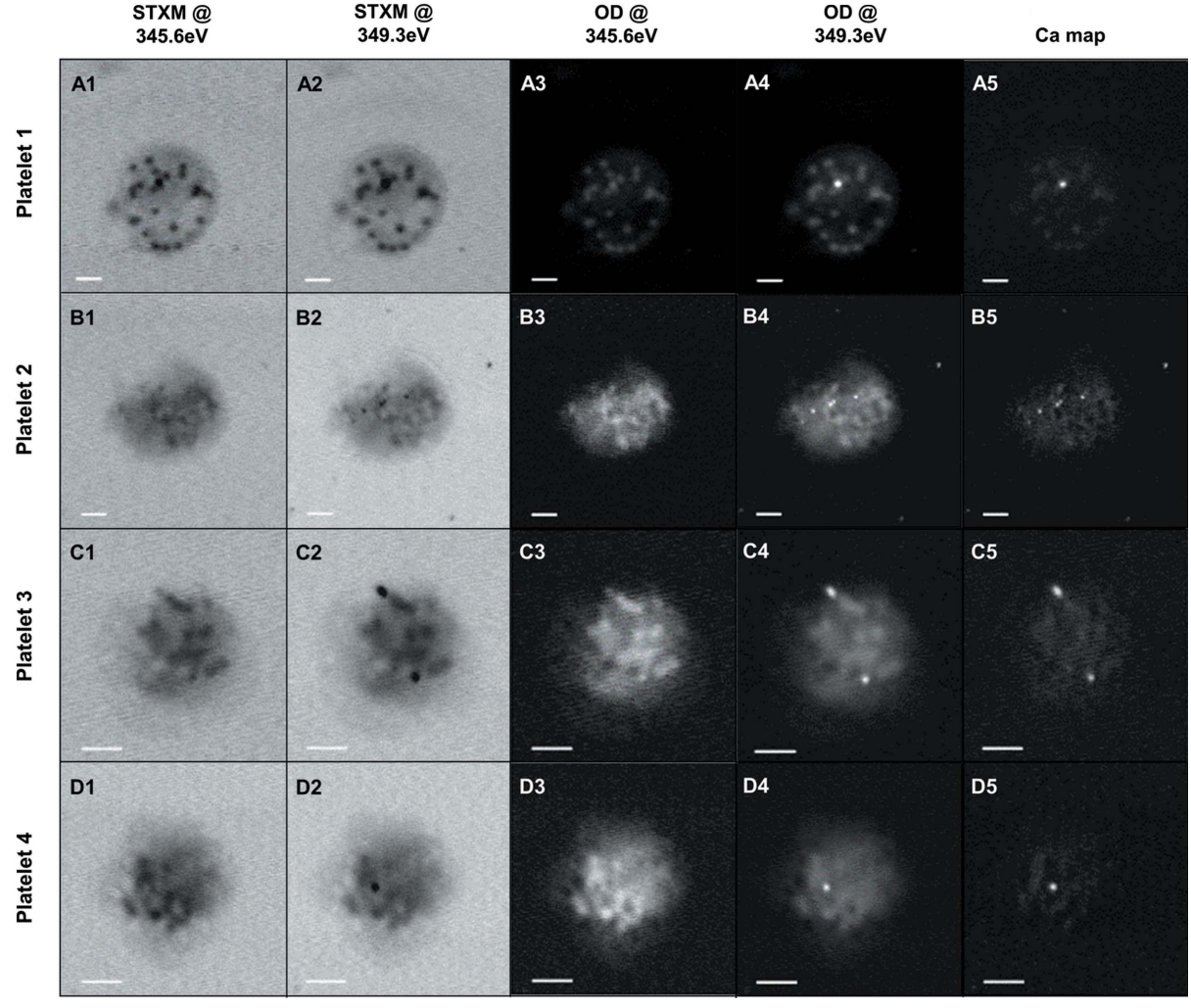

Figure 3
STXM transmission images at (A1–D1) 345.6 eV and (A2–D2) 349.3 eV. STXM OD images at (A3–D3) 345.6 eV and (A4–D4) 349.3 eV. (A5–D5) Calcium maps for four platelets, 1–4. Scale bars are 1 μm.

numbers of platelets could provide statistically meaningful criteria for these purposes.

We believe that our study has shown the potential capabilities of STXM to identify and count DGs as a complementary method to the typical WM TEM approach. Furthermore, STXM also has the potential for semi-quantitative Ca-content estimation and chemical species-specific maps, which may further improve the accuracy of DGD diagnosis. Additionally, it should be noted that this study is a proof of concept for the diagnosis of DGD, rather than for actual clinical use, since synchrotron facilities and STXM beamlines are currently not available for practical clinical applications. However, since the development of laboratory-based X-ray sources and tabletop instruments for this purpose is actively in progress (Raj *et al.*, 2018; Zhang *et al.*, 2018; Hall & Lewis, 2019), our study may provide a basis for future clinical applications.

4. Conclusions

In conclusion, an X-ray spectromicroscopic technique (*i.e.* STXM) has been adapted to identify and count DGs in human platelets, and its promising capability in this application has been demonstrated. Its element-specific contrast mechanism based on differences in X-ray absorption edge allows us to distinguish Ca-rich DGs more clearly from the other subcellular components.

We would like to propose STXM as a promising approach for DGD diagnosis with an improved identification and counting capability, which complements the current WM TEM method.

Acknowledgements

We would like to thank Dr Namdong Kim, Dr Hyun-Joon Shin and Ms Mikang Kim of Pohang Light Source for their assistance on the STXM beamline.

Funding information

The following funding is acknowledged: National Research Foundation of Korea, Ministry of Science and ICT (grant No. 2017M3A9G8084539) and (grant No. 2017K1A3A7A-09016394).

References

Benzerara, K., Yoon, T. H., Tyliszczak, T., Constantz, B., Spormann, A. M. & Brown, G. E. (2004). *Geobiology*, **2**, 249–259.

Brunet, J. G., Iyer, J. K., Badin, M. S., Graf, L., Moffat, K. A., Timleck, M., Spitzer, E. & Hayward, C. P. M. (2018). *Int. J. Lab. Hematol.* **40**, 400–407.

Chen, D., Uhl, C. B., Bryant, S. C., Krumwiede, M., Barness, R. L., Olson, M. C., Gossman, S. C., Erdogan Damgard, S., Gamb, S. I., Cummins, L. A., Charlesworth, J. E., Wood-Wentz, C. M., Salisbury, J. L., Plumhoff, E. A., Van Cott, E. M., He, R., Warad, D. M., Pruthi, R. K., Heit, J. A., Nichols, W. L. & White, J. G. (2018). *Platelets*, **29**, 574–582.

Cosmidis, J., Benzerara, K., Nassif, N., Tyliszczak, T. & Bourdelle, F. (2015). *Acta Biomater.* **12**, 260–269.

Fleet, M. E. & Liu, X. (2009). *Am. Mineral.* **94**, 1235–1241.

Hall, C. & Lewis, R. (2019). *Philos. Trans. R. Soc. A.* **377**, 20180240.

Hayward, C. P., Moffat, K. A., Plumhoff, E., Timleck, M., Hoffman, S., Spitzer, E., Van Cott, E. M. & Meijer, P. (2012). *Semin. Thromb. Hemost.* **38**, 622–631.

Hayward, C. P., Moffat, K. A., Spitzer, E., Timleck, M., Plumhoff, E., Israels, S. J., White, J. & NASCOLA Working Group on Platelet Dense Granule Deficiency (2009). *Am. J. Clin. Pathol.* **131**, 671–675.

Hitchcock, A. P. (2019). *aXis2000*, http://unicorn.mcmaster.ca/aXis2000.html.

Introne, W., Boissy, R. E. & Gahl, W. A. (1999). *Mol. Genet. Metab.* **68**, 283–303.

Israels, S. J., Gerrard, J. M., Jacques, Y. V., McNicol, A., Cham, B., Nishibori, M. & Bainton, D. F. (1992). *Blood*, **80**, 143–152.

Kwon, D., Nho, H. W. & Yoon, T. H. (2014). *Colloids Surf. B Biointerfaces*, **122**, 384–389.

Lo, B., Li, L., Gissen, P., Christensen, H., McKiernan, P. J., Ye, C., Abdelhaleem, M., Hayes, J. A., Williams, M. D., Chitayat, D. & Kahr, W. H. (2005). *Blood*, **106**, 4159–4166.

McNicol, A. & Israels, S. J. (1999). *Thromb. Res.* **95**, 1–18.

Naftel, S. J., Sham, T. K., Yiu, Y. M. & Yates, B. W. (2001). *J. Synchrotron Rad.* **8**, 255–257.

Nelson, J., Huang, X., Steinbrener, J., Shapiro, D., Kirz, J., Marchesini, S., Neiman, A. M., Turner, J. J. & Jacobsen, C. (2010). *Proc. Natl Acad. Sci. USA*, **107**, 7235–7239.

Nho, H. W., Kalegowda, Y., Shin, H. J. & Yoon, T. H. (2016). *Sci. Rep.* **6**, 24488.

Nho, H. W. & Yoon, T. H. (2017). *Sci. Rep.* **7**, 1–10.

Nishibori, M., Cham, B., McNicol, A., Shalev, A., Jain, N. & Gerrard, J. M. (1993). *J. Clin. Invest.* **91**, 1775–1782.

Obst, M., Dynes, J. J., Lawrence, J. R., Swerhone, G. D. W., Benzerara, K., Karunakaran, C., Kaznatcheev, K., Tyliszczak, T. & Hitchcock, A. P. (2009). *Geochim. Cosmochim. Acta*, **73**, 4180–4198.

Raj, V. A., Sharma, S., Misra, R., Mishra, R., Pankaj, P., Garg, A. & Singh, M. (2018). *J. Anal. Pharm. Res.* **7**, 175–180.

Rieger, D., Himpsel, F. J., Karlsson, U. O., McFeely, F. R., Morar, J. F. & Yarmoff, J. A. (1986). *Phys. Rev. B*, **34**, 7295–7306.

Ruiz, F. A., Lea, C. R., Oldfield, E. & Docampo, R. (2004). *J. Biol. Chem.* **279**, 44250–44257.

White, J. G. (1969). *Blood*, **33**, 598–606.

White, J. G. (1979). *Am. J. Pathol.* **95**, 445–462.

White, J. G. (1998). *Semin. Thromb. Hemost.* **24**, 163–168.

White, J. G. (2004). *Electron Microscopy Methods for Studying Platelet Structure and Function*. *Platelets and Megakaryocytes*, Vol. 1, *Functional Assays*, edited by J. N. Gibbins & M. P. Mahout-Smith, pp. 47–63. Totowa, New Jersey, USA: Humana Press.

Yang, N., Nho, H. W., Kalegowda, Y., Kim, J. B., Song, J., Shin, H. & Yoon, T. H. (2014). *Bull. Korean Chem. Soc.* **35**, 2625–2629.

Zhang, R., Li, L., Sultanbawa, Y. & Xu, Z. P. (2018). *Am. J. Nucl. Med. Mol. Imaging*, **8**, 169–188.